VIII. MICROWAVE ELECTRONICS*

Prof. L. D. Smullin
Prof. H. A. Haus
Prof. A. Bers
D. L. Morse
R. B. McCullough
W. R. Rummler
W. K. Rushforth

RESEARCH OBJECTIVES

We shall continue our work on the theory of wideband, high-power klystrons, and on wideband circuits for klystrons and traveling-wave tubes.

1. We shall be studying multigap, klystron output cavities in an attempt to realize bandwidth of 20 per cent at the megawatt power level.
2. The wideband-buncher klystron analysis will be extended to other configurations than the one illustrated in this report.
3. The X-line will be studied experimentally to determine its applicability to high-power traveling-wave amplifiers at one extreme, and to millimeter tubes at the other.

L. D. Smullin

A. BROADBAND-BUNCHER KLYSTRON

W. H. Watson and R. E. Holady (1), of Litton Industries, Inc., have described a novel wideband klystron which they call the "Skirtron." This is shown in Fig. VIII-1, in which the frequency responses of the various cavities are indicated.

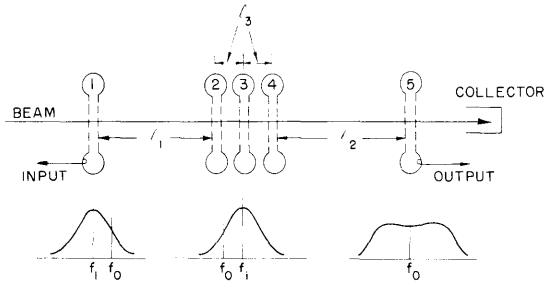

Fig. VIII-1. Schematic of "Skirtron" wideband klystron.

The input cavity (No. 1) is a simple resonant circuit, very heavily loaded by the input circuit, and tuned to a resonant frequency $f_1 < f_o$, where f_o designates the center of the frequency band that is of interest. The intermediate cavities are located at a distance $\ell_1 \approx \lambda_q/2$ beyond the input cavity, where λ_q is the effective plasma wavelength in the beam. Each of these is tuned to a common frequency $f_i > f_o$. They are heavily loaded by resistive loss, are not coupled electromagnetically, and are spaced a distance $\ell_3 \approx \lambda_q/20$ apart. The output cavity is located $\ell_2 \approx \lambda_q/4$ beyond the last intermediate cavity. It is of a wideband variety, having a passband centered on f_o. (The design of such an output cavity is still a serious problem, but that matter is not a part of this discussion.)

The over-all frequency response of such a tube is reported to be very flat over a bandwidth of 10 per cent, or so, while the gain remains fairly high, approximately 30 db.

*This research was supported in part by Purchase Order DDL-B222 with Lincoln Laboratory, a center for research operated by M.I.T., which is supported by the U.S. Air Force under Air Force Contract AF19(604)-5200; and in part by the U.S. Navy (Office of Naval Research) under Contract Nonr-1841(49). Reproduction in whole or in part is permitted for any purpose of the United States Government.

Watson and Holady (1) say that the flat bandwidth results from the multiplication of the complementary skirts of the input and intermediate cavity characteristics, whence the name "Skirtron." They have not made it clear why the gain is so high with the cavities so heavily loaded. The spacings ℓ_1 are small, and $\ell_2 \approx \lambda_q/4$ is the distance to the output cavity.

We have carried out a small-signal, space-charge wave analysis of this configuration. Our analysis actually predicts large gain and bandwidth, which is in agreement with their experiments. It is possible, also, to reduce the length of the first drift-tube from $\ell_1 \approx \lambda_q/2$ to $\ell_1 \approx \ell_3 = \lambda_q/20$ without substantially affecting the tube performance.

Consider the system shown in Fig. VIII-2. If the cavity gaps are short, $\theta_g \ll 1$, we can assume that the beam leaving the input gap carries an ac kinetic voltage $U_1 = -MV_1$, where $M \approx 1$ is the gap coupling coefficient, and V_1 is the gap voltage. The convection current at this plane may be ignored (a good approximation).

The group of intermediate cavities may be treated as a multigap klystron (1, 2). Or, if these cavities are assumed to be very close together, the system will behave like a reactive-medium amplifier (Easytron). In the second case, with many intermediate cavities very close together, the beam emerges with relatively large velocity modulation as compared with the current modulation. We have

$$\frac{U_n}{J_n Z_o} = \frac{1}{\left(1 - \frac{\omega_i^2}{\omega^2} - \frac{j\omega}{\omega_i Q_i}\right)^{1/2}}$$

where $Z_o = (2V_o/I_o)(\omega_q/\omega)$, ω_i is the intermediate-cavity resonant frequency, and Q_i is the Q of the cavities. For ω in the neighborhood of ω_i, $U_n/J_n Z_o \gg 1$.

The gain of the continuous intermediate section goes as $U_n \propto U_1 e^{\alpha z}$, where

$$\alpha = \mathrm{Re}\left[\frac{j\beta_{pe}}{\left(1 - \frac{\omega_i^2}{\omega^2} - j\frac{\omega}{\omega_i Q_i}\right)^{1/2}}\right]$$

Figure VIII-3 is a qualitative plot of the gain versus frequency for lossless, and lossy, continuous intermediate structures, and for a structure consisting of a finite number of cavities with small, but nonzero, spacing (ℓ_1). The gain of such a structure may be very high, even with heavy loading (low Q_i).

Calculations were made of the small-signal gain of a hypothetical tube with the following characteristics:

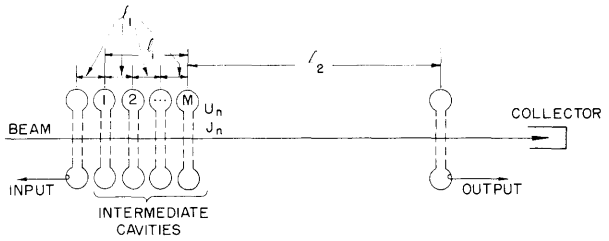

Fig. VIII-2. Wideband-buncher klystron.

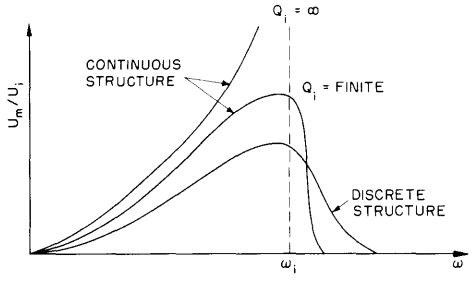

Fig. VIII-3. Gain-frequency characteristics of continuous (Easytron) resonant structures and discrete structures.

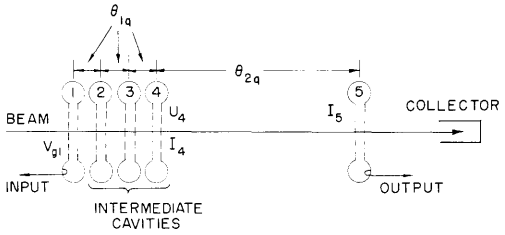

Fig. VIII-4. Wideband-buncher klystron.

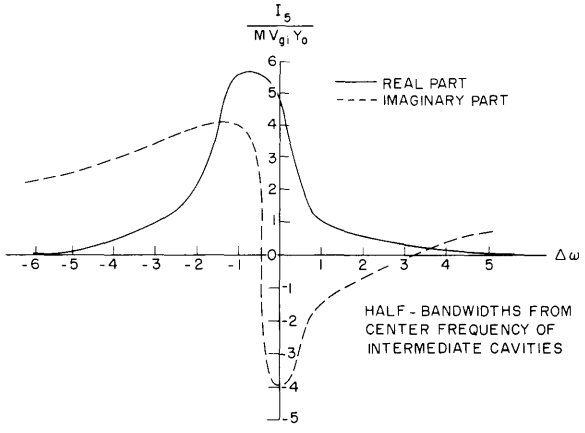

Fig. VIII-5. Real and imaginary parts of beam current (I_5) at the output cavity.

V_o = 140 kv — Gap transit angle, $\beta_e d = 0.5$

I_o = 71 amps — Gap radius, $\beta_e r = 0.63$

$P_o = 10^7$ watts — R/Q = 70

λ_o = 25 cm — $R_{shunt} = 5.5 \times 10^5$ ohms

λ_q = 145 cm — Cavity spacing $\begin{cases} \ell_1 = 0.05\,\lambda_q \\ \theta_1 = 2\pi\ell_1/\lambda_q \end{cases}$

Input cavity loaded to $Q_L = 10$ by the source

Three intermediate cavities loaded to $Q_L = 10$ by loss

The beam excitation at the output of the last idler cavity in Fig. VIII-4 can be shown (2) to be

$$\frac{U_4}{MV_1} = \left[1 - j6(\theta_1 z) - 5(\theta_1 z)^2 + j(\theta_1 z)^3\right]$$

$$\frac{I_4}{Y_o M V_1} = \left[j3\theta_1 + 4\theta_1(\theta_1 z) - j\theta_1(\theta_1 z)^2\right]$$

where $z = \left(M_i^2 Z_i\right)/Z_o$; $M_i = 1$ is the intermediate gap coupling coefficient; Z_i, is the impedance of loaded, intermediate cavities; and Z_o is the characteristic impedance of the electron beam.

The ac current, I_5, was found to have a maximum amplitude at a distance $\theta_{2q} = 74°$ beyond the last intermediate cavity. The real and imaginary parts of I_5 versus ω are shown in Fig. VIII-5.

The output power of the tube is given by

$$P_L = \frac{|I_5|^2}{2G_L} = \frac{|I_5|^2}{2G_o} = \frac{|y_5|^2\,|V_1|^2}{2G_o}$$

where G_L is the load conductance, assumed to be equal to the beam conductance; $G_o = I_o/V_o$, and y_5 is a transadmittance relating V_1 and I_5. The input power to the tube is given by

$$P_{in} = \frac{|V_1|^2}{2}(G_{sh} + G_{e\ell})$$

In order to load the input cavity to a very low Q, the generator conductance must be very large, and there is a large reflection mismatch. Thus the available gain is defined as

$$G = \frac{\text{Power out of tube}}{\text{Available generator power}} \qquad G = \frac{|y_5(\omega)|^2}{4}\left(\frac{G_{sh} + G_{e\ell}}{G_o}\right) \cdot L_1(\omega)$$

where L_1 is the input reflection loss ($0 < L_1 < 1$). For the case considered, L_1 was -18 db

at the input-cavity resonant frequency.

Figure VIII-6a shows a curve computed with the input cavity tuned 3 half-bandwidths

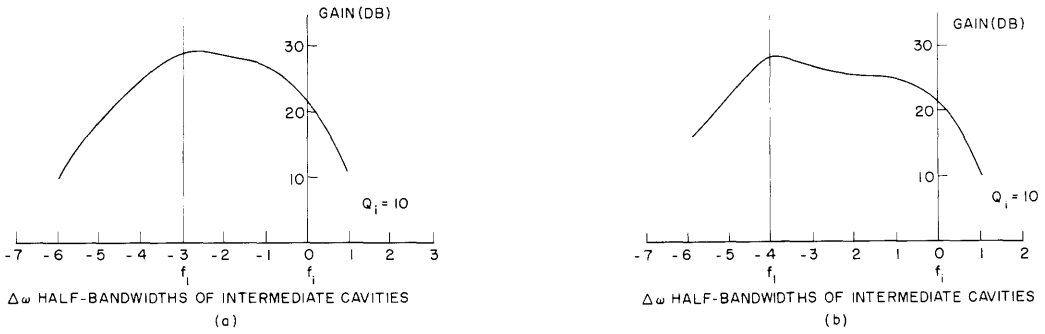

Fig. VIII-6. Gain-frequency characteristic of wideband-buncher klystron with input cavity tuned to f_l and idler cavities to f_i.

below the intermediate cavities. A bandwidth of approximately 15 per cent, and a gain of approximately 29 db, are indicated. In Fig. VIII-6b, the input cavity is tuned 4 half-bandwidths below f_i. It can be seen that decreasing the bandwidth of the intermediate cavities somewhat (raising their gain at $\Delta f = 0$) would result in a fairly flat response over a bandwidth of approximately 20 per cent.

When the input gap is lengthened to $\theta_{gl} = 2$, the electronic loading $G_{e\ell}$ is increased, and an ac current is induced at the output of the input gap. This current does not appreciably affect the ratio I_5/V_{gi}, but allows a much better power match at the input cavity.

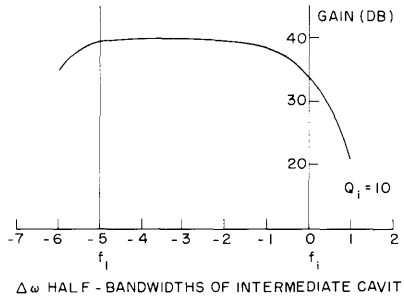

Fig. VIII-7. Gain-frequency characteristic of wideband-buncher klystron with input cavity tuned to f_l and idler cavities to f_i. Transit angle of input gap is increased to 2 radians to make $G_{e\ell}$ appreciable.

The effect is a shifting of the whole gain curve upward, which allows greater separation in frequency of the input and intermediate cavities and still maintains acceptable gain.

The calculated gain versus bandwidth curve for the input cavity ($Q_{input} = 6\ 2/3$) tuned

5 half-bandwidths below the intermediate cavities is shown in Fig. VIII-7. The peak gain is approximately 39 db, and the bandwidth is very nearly 6 half-bandwidths of an intermediate cavity, or approximately 30 per cent.

L. D. Smullin, D. L. Morse

References

1. W. H. Watson and R. E. Holady, a paper presented at the 1959 Electron Devices Meeting, Washington, D.C., Oct. 29-30, 1959 (unpublished).

2. A. Bers, Interaction of electrons with electromagnetic fields of gaps with application to multicavity klystrons, Sc.D. Thesis, Department of Electrical Engineering, M.I.T., June 1959.

B. SPACE-CHARGE MODE THEORY OF MULTICAVITY KLYSTRONS

In Quarterly Progress Report No. 55, pages 65-70, we presented the theory of interaction between an electron stream and the electromagnetic fields of a gap. The multicavity klystron will be considered to consist of a succession of such gaps. Except for the electron stream, the gap circuits will be assumed to be uncoupled.

The gap interaction can be summarized in the convenient matrix form

$$\begin{bmatrix} \underline{\underline{B}}_{II} \\ I_g \end{bmatrix} = \left[\begin{array}{c|c} \underline{\underline{D}}_{I,II} & \underline{\underline{D}}_{gII} \\ \hline \underline{\underline{\Gamma}}_g \underline{\underline{D}}_{Ig} & Y_{e\ell} \end{array}\right] \begin{bmatrix} \underline{\underline{B}}_{I} \\ V_g \end{bmatrix} \tag{1}$$

where I, II, and g refer to reference planes as shown in Fig. VIII-8, and, in the notation of the previous report (1),

$$\underline{\underline{B}} = \begin{bmatrix} \underline{\underline{B}}^{(1)} \\ \vdots \\ \underline{\underline{B}}^{(n)} \end{bmatrix}; \quad \underline{\underline{B}}^{(k)} = \begin{pmatrix} V_k \\ I_k \end{pmatrix} \tag{2}$$

$$\underline{\underline{D}} = \begin{bmatrix} \underline{\underline{D}}^{(1)} & & \bigcirc \\ & \ddots & \\ \bigcirc & & \underline{\underline{D}}^{(n)} \end{bmatrix}; \quad \underline{\underline{D}}^{(k)} = \left[\begin{array}{c|c} \cos\theta_k & jZ_{ok}\sin\theta_k \\ \hline jY_{ok}\sin\theta_k & \cos\theta_k \end{array}\right] e^{-j\theta_e} \tag{3}$$

$$\underline{\underline{K}}_g = \begin{bmatrix} \underline{\underline{K}}_g^{(1)} \\ \vdots \\ \underline{\underline{K}}_g^{(n)} \end{bmatrix}; \quad \underline{\underline{K}}_g^{(k)} = \begin{pmatrix} M_k \\ Y_{ok}\, N_k \end{pmatrix} \tag{4}$$

$$M_k = \frac{1}{2}\left(M_{+k} + M_{-k}\right) C_k \tag{5}$$

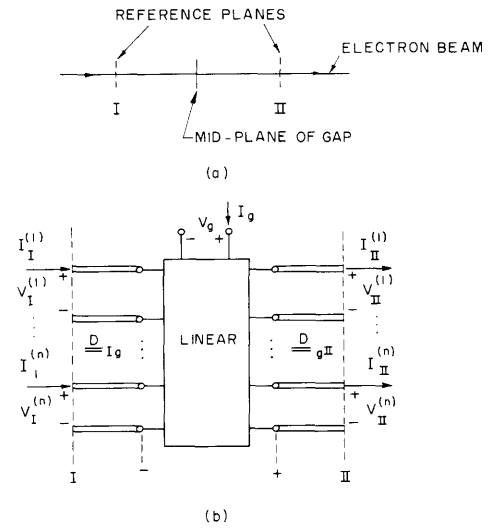

Fig. VIII-8. Schematic representation of the gap region of interaction: (a) reference planes in the gap region; planes I and II are located where the gap fields are zero; (b) multiport representation of the interaction; the independent transmission lines represent the diagonal drift transformations. Planes (-) and (+) are, respectively, just at the left and right of g.

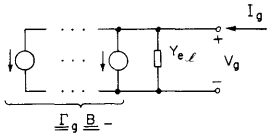

Fig. VIII-9. Equivalent circuit at the gap terminals.

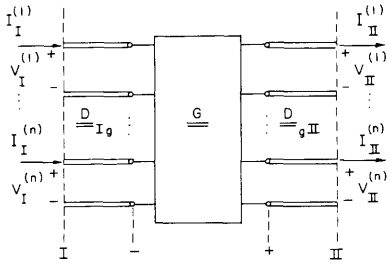

Fig. VIII-10. Equivalent circuit in the beam when $I_g = -Y_c V_g$.

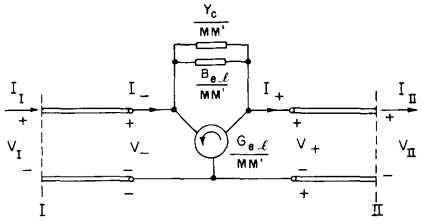

Fig. VIII-11. Equivalent circuit in the beam for a single-mode transformation through a symmetric gap.

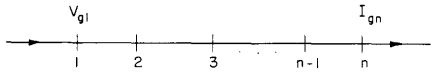

Fig. VIII-12. Schematic representation of multicavity klystron. The location of the mid-plane of each gap is shown.

$$N_k = \frac{1}{2}(M_{+k} - M_{-k})\, C_k \tag{6}$$

$$\underline{\underline{\Gamma}}_g = \left[\underline{\underline{\Gamma}}_g^{(1)} \ldots \underline{\underline{\Gamma}}_g^{(n)}\right]; \quad \underline{\underline{\Gamma}}_g^{(k)} = (Y_{ok}\, N'_k \qquad M'_k) \tag{7}$$

$$M'_k = \frac{1}{2}\left(M^*_{+k} + M^*_{-k}\right) K_k \tag{8}$$

$$N'_k = \frac{1}{2}\left(M^*_{+k} - M^*_{-k}\right) K_k \tag{9}$$

The superscripts 1 ... k ... n and subscript k refer to the various space-charge modes, and $Y_{e\ell}$ has been defined previously (1). The formulation of Eqs. 1-9 places in evidence the importance of choosing the mid-plane of the gap as a reference. Equation 1 can be rewritten

$$\begin{bmatrix} \underline{\underline{B}}_{II} \\ I_g \end{bmatrix} = \begin{bmatrix} \underline{\underline{D}}_{gII} & 0 \\ 0 & 1 \end{bmatrix} \begin{bmatrix} \underline{\underline{I}} & \underline{\underline{K}}_g \\ \underline{\underline{\Gamma}}_g & Y_{e\ell} \end{bmatrix} \begin{bmatrix} \underline{\underline{D}}_{Ig} & 0 \\ 0 & 1 \end{bmatrix} \begin{bmatrix} \underline{\underline{B}}_I \\ V_g \end{bmatrix} \tag{10}$$

which has the drift and gap parameters separated as shown in Fig. VIII-1b.

a. The Equivalent Circuit at the Gap

From Eq. 1, the short-circuit gap current is

$$I_g\big|_{V_g=0} = \underline{\underline{\Gamma}}_g \underline{\underline{B}}_- = \sum_k (Y_o N' V_- + M' I_-)^{(k)} \tag{11}$$

where the subscript (minus) denotes the plane just preceding the mid-plane of the gap. The gap circuit is loaded by $Y_{e\ell}$. The real part of $Y_{e\ell}$ is given by

$$G_{e\ell} = \frac{1}{4}\sum_k Y_{ok}\left[|M_{+k}|^2 - |M_{-k}|^2\right] C_k K_k \tag{12}$$

The imaginary part of $Y_{e\ell}$ is, similarly, a sum of $B_{e\ell k}$ over all the modes (1). The equivalent circuit at the gap terminals is shown in Fig. VIII-9.

b. Equivalent Circuit in the Beam

When the gap circuit is representable by an admittance Y_c, then

$$I_g = -Y_c V_g \tag{13}$$

The transformation of the excitation in the beam is found from Eqs. 1 and 13:

$$\underline{\underline{B}}_{II} = \left[\underline{\underline{D}}_{gII}\, \underline{\underline{G}}\, \underline{\underline{D}}_{Ig}\right] \underline{\underline{B}}_I \tag{14}$$

where

$$\underline{\underline{G}} = \underline{\underline{I}} + \underline{\underline{K}}_g(-Z_g)\,\underline{\underline{\Gamma}}_g \tag{15}$$

$$Z_g = \frac{1}{Y_c + Y_{e\ell}} \tag{16}$$

and $\underline{\underline{I}}$ is the identity matrix. The mixing of the modes, which occurs because of the gap, is contained in the matrix

$$\underline{\underline{K}}_g\,\underline{\underline{\Gamma}}_g = \begin{bmatrix} \underline{\underline{K}}_g^{(1)}\underline{\underline{\Gamma}}_g^{(1)} & \cdots & \underline{\underline{K}}_g^{(1)}\underline{\underline{\Gamma}}_g^{(n)} \\ \vdots & & \vdots \\ \underline{\underline{K}}_g^{(n)}\underline{\underline{\Gamma}}_g^{(1)} & \cdots & \underline{\underline{K}}_g^{(n)}\underline{\underline{\Gamma}}_g^{(n)} \end{bmatrix} \tag{17}$$

where

$$\underline{\underline{K}}_g^{(i)}\underline{\underline{\Gamma}}_g^{(j)} = \left[\begin{array}{c|c} Y_{oj}\,N_j'\,M_i & M_j'\,M_i \\ \hline Y_{oj}\,N_j'\,Y_{oi}\,N_i & Y_{oi}\,N_i\,M_j' \end{array}\right] \tag{18}$$

The equivalent circuit for Eq. 14 is shown in Fig. VIII-10.

For a single mode, Eq. 15 becomes simply

$$\underline{\underline{G}} = \left[\begin{array}{c|c} 1 - Y_o MN'\,Z_g & -MM'\,Z_g \\ \hline -Y_o^2 N'\,NZ_g & 1 - Y_o M'\,NZ_g \end{array}\right] \tag{19}$$

If the gap is symmetric [that is, (M/C) = (M'/K) and (N/C) = (N'/K)], the equivalent circuit for Eq. 14 is a loaded gyrator, as shown in Fig. VIII-11. This was pointed out by R. B. McCullough.

c. Multicavity Klystrons

i. Cascade formulation

The schematic of a multicavity klystron is shown in Fig. VIII-12. It consists of a succession of gaps of arbitrary characteristics. The gain of the multicavity klystron is proportional to the transfer admittance I_{gn}/V_{g1}, which can be written with the aid of Eqs. 1, 4, 7, and 14.

$$\frac{I_{gn}}{V_{g1}} = \underline{\underline{\Gamma}}_{gn}\,\underline{\underline{D}}_{n-1,n}\,\underline{\underline{G}}_{n-1}\,\underline{\underline{D}}_{n-2,n-1}\,\underline{\underline{G}}_{n-2}\cdots\underline{\underline{D}}_{23}\,\underline{\underline{G}}_2\,\underline{\underline{D}}_{12}\,\underline{\underline{K}}_{g1} \tag{20}$$

ii. Two-gap transfer admittance

Consider two gaps as shown below:

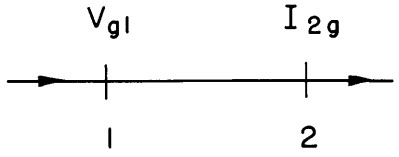

Let

$$I_{2g} = -I_{g2}\Big|_{V_{g2}=0}; \quad V_{g2} = I_{2g} Z_2 \tag{21}$$

where Z_2 is as defined by Eq. 16. We define the two-gap transfer admittance

$$y_{21} = \frac{I_{2g}}{V_{g1}} = -\underline{\underline{\Gamma}}_2 \underline{\underline{D}}_{12} \underline{\underline{K}}_1 \tag{22}$$

With the use of Eqs. 2-9, Eq. 22 becomes

$$y_{21} = -\exp(-j\theta_{e1,2}) \sum_k [Y_o(M_1 N_2' + M_2' N_1) \cos\theta_{12} + jY_o(M_1 M_2' + N_1 N_2') \sin\theta_{12}]^{(k)} \tag{23}$$

The subscripts could, clearly, apply to any two gaps.

iii. Feedforward formulations

A different approach to the determination of the multicavity klystron gain is to consider the output as a linear combination of the outputs resulting from excitations in all the gaps. If we consider that the outputs are the result of the two main signal transfer mechanisms in the device – drifting and interaction with gap fields – we can write the transfer functions for any number of gaps by inspection. For example, the transfer admittance for a three-cavity klystron,

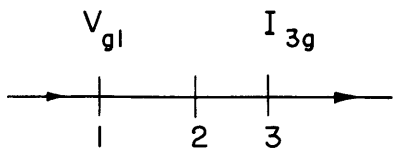

is given by

$$\frac{I_{3g}}{V_{g1}} = y_{21}y_{32}Z_2 + y_{31} \tag{24}$$

We note that the first term is an interaction, or cascade, term, the second is a drift, or feedforward, term. Similarly, for a four-cavity klystron,

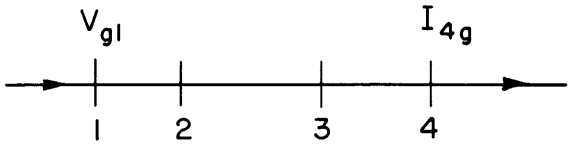

the transfer admittance is given by

$$\frac{I_{4g}}{V_{g1}} = y_{21}y_{32}y_{43}Z_2Z_3 + y_{31}y_{43}Z_3 + y_{21}y_{42}Z_2 + y_{41} \tag{25}$$

The excitation in the beam at any plane can also be found by inspection. For example, the beam excitation after four gaps,

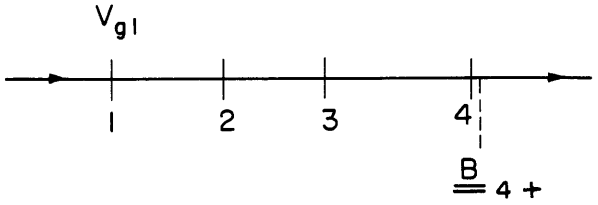

is given by

$$\begin{aligned}\frac{\underline{\underline{B}}_{4+}}{V_{g1}} = {} & \underline{\underline{K}}_4[y_{21}y_{32}y_{43}Z_2Z_3Z_4] + \underline{\underline{K}}_4[y_{31}y_{43}Z_3Z_4] + \underline{\underline{K}}_4[y_{21}y_{42}Z_2Z_4] \\ & + \underline{\underline{D}}_{43}\underline{\underline{K}}_3[y_{21}y_{32}Z_2Z_3] + \underline{\underline{K}}_4[y_{41}Z_4] + \underline{\underline{D}}_{43}\underline{\underline{K}}_3[y_{31}Z_3] \\ & + \underline{\underline{D}}_{42}\underline{\underline{K}}_2[y_{21}Z_2] + \underline{\underline{D}}_{41}\underline{\underline{K}}_1\end{aligned} \tag{26}$$

In general, for an n-cavity klystron, by the feedforward formulation, we have

$$\frac{I_{ng}}{V_{g1}} = \sum_k \sum_k \prod_k y_{(k+1),(k-1)} \prod_{p=2}^{n-1} {}^{k}\, y_{p,(p-1)}\, Z_p \tag{27}$$

where the first sum is over all possible types of k, that is, k = 0, k = 2, 3 ... n - 1, k = all pairs, k = all triplets, etc., k = all intermediate gaps; the second sum is a cyclic permutation over all the k's of one type; Π denotes a product, and Π^k denotes a product with the k^{th} member missing.

A. Bers

References

1. A. Bers, Space-charge mode theory of gap interaction, Quarterly Progress Report No. 55, Research Laboratory of Electronics, M.I.T., Oct. 15, 1959, p. 65.

C. THE X-LINE SLOW-WAVE STRUCTURE

The X-line is a periodic structure consisting of wires or bars across a circular tube. The wires are alternately rotated back and forth through an angle α, as shown in Fig. VIII-13 (if $\alpha = 0$ we have a simple ladder line). The phase shift per section was first determined by cold measurements, and later by beam probe measurements. The cold tests consisted of measurements of the resonances of structures having various numbers of wires. Some idea of the field configuration was obtained by observing the shift of resonant frequency as a small metal bead was pulled through the structure, either along the axis or on some line parallel to it.

Except for the case when $\alpha = 0$, this structure has no transverse planes of symmetry. Therefore it is not possible to measure the resonances of an elementary cell, and thereby deduce the upper and lower cutoff frequencies of the various passbands. In this respect, it resembles an interdigital line. An experimental determination of the $\omega - \beta$ diagram must be made with a large enough number of elements to make the end effects unimportant. Figure VIII-14 shows the natural frequencies of resonators consisting of various numbers of wires, with $\alpha = 90°$. It is clear that 6 pairs give the cutoff frequencies with very good accuracy. Figure VIII-15 is an $\omega - \beta$ plot for the nine-pair resonator, taken from the data of Fig. VIII-14. A striking feature of the $\omega - \beta$ diagram is the large angle with which the curve appears to approach the upper and lower cutoff points.

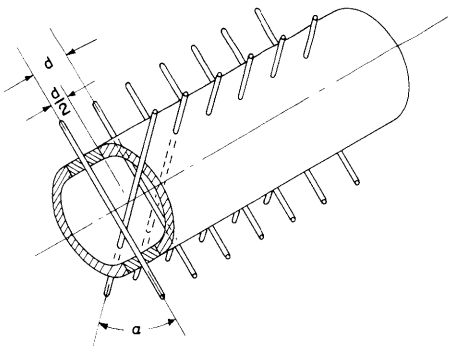

Fig. VIII-13. Elementary X-line structure.

Figure VIII-16 illustrates the effect of varying the angle, α, between the wires, from

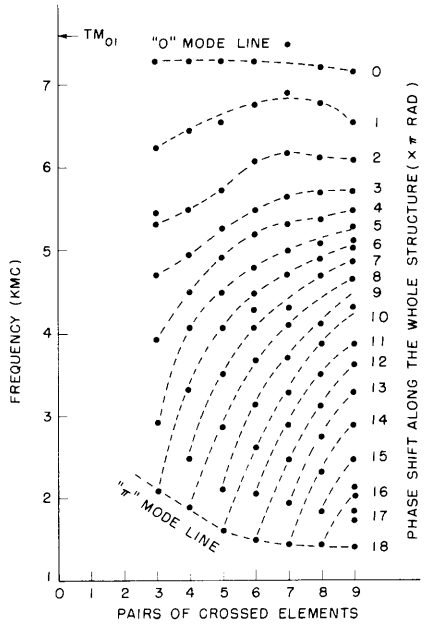

Fig. VIII-14. Resonances of an X-line structure (α=90°) versus number of pairs of crossed wires.

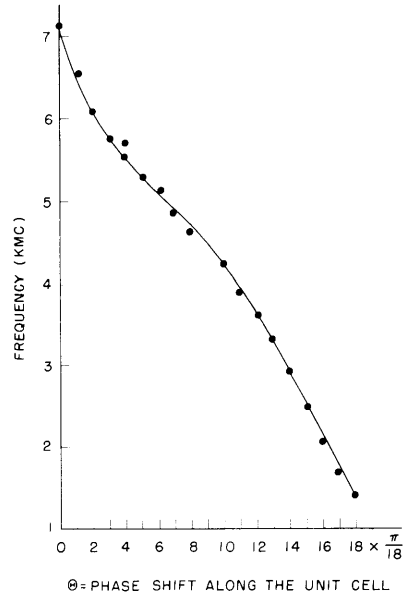

Fig. VIII-15. $\omega - \beta$ diagram of X-line (α=90°).

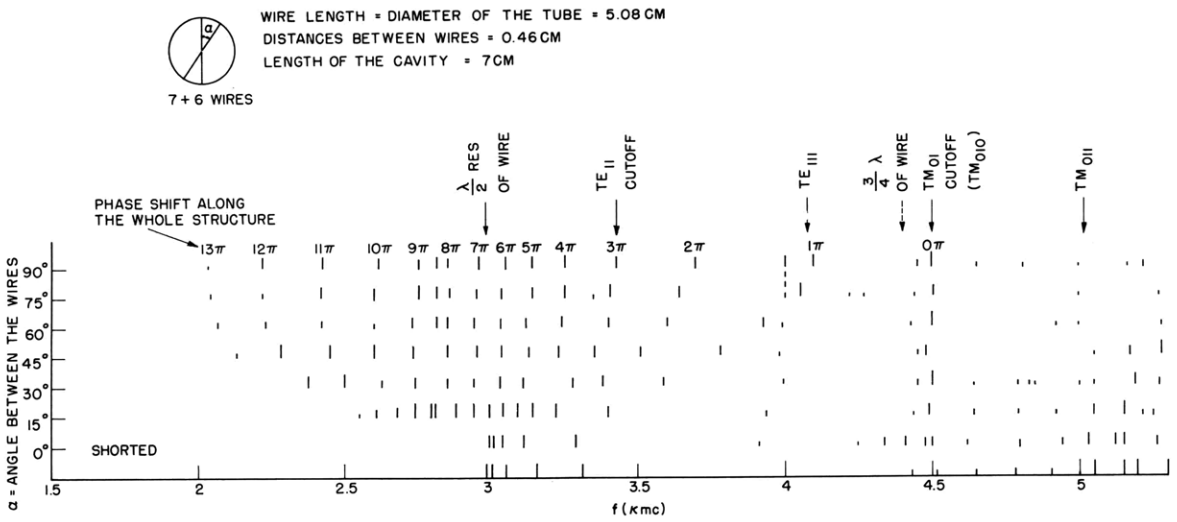

Fig. VIII-16. Effect of angle α on resonant-frequency pattern of X-line.

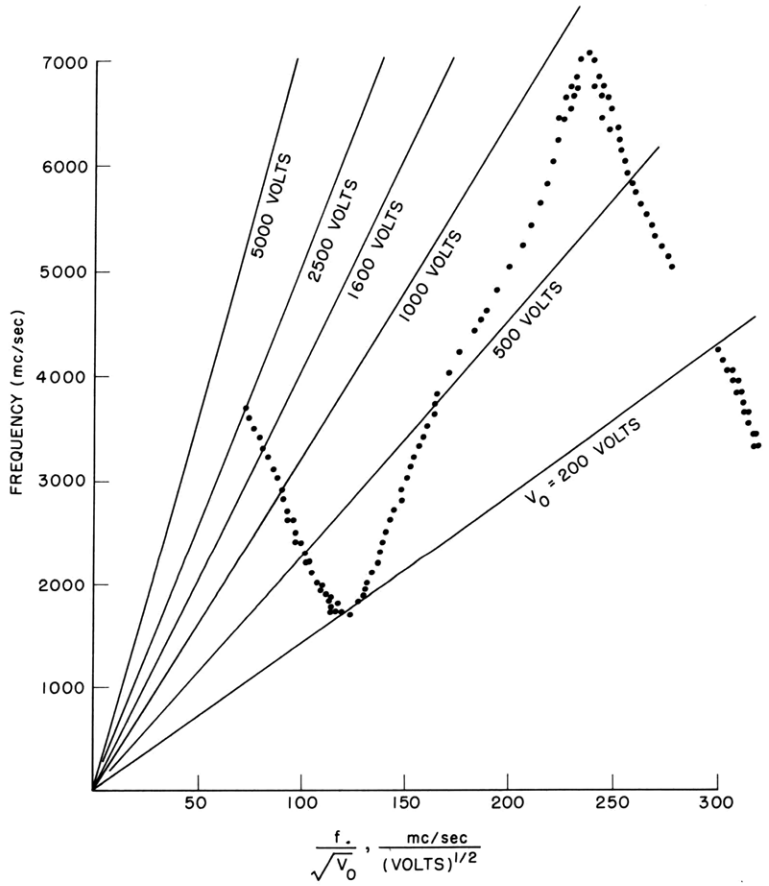

Fig. VIII-17. $\omega - \beta$ diagram of X-line determined by electron-beam interaction.

0° to 90°. The structure that was measured had 13 wires. It will be observed that this structure has a fundamental backward-wave space harmonic, and thus should be suitable for use as a backward-wave oscillator. The advantage of this structure over the simple ladder line lies in its much greater bandwidth.

Dr. R. C. Hergenrother, of the Spencer Laboratories, Raytheon Corporation, has constructed an X-line backward-wave oscillator. He has kindly loaned it to us to make electron-beam interaction measurements of the $\omega - \beta$ diagram (1). The beam is operated well below the starting current for backward-wave oscillation (<1 ma). At some fixed input frequency, the beam voltage is varied and points at which the rf output power changes are noted, and plotted as in Fig. VIII-17.

L. D. Smullin, W. R. Rummler, R. Litwin

References

1. D. A. Watkins and A. E. Siegman, Helix impedance measurements using an electron beam, J. Appl. Phys. 24, 917-922 (1953).